

# Predictions for $\sqrt{s} = 200 \text{ A}\cdot\text{GeV}$ Au+Au Collisions from Relativistic Hydrodynamics

B.R. Schlei<sup>1,2\*</sup> and D. Strottman<sup>2†</sup>

<sup>1</sup>*Physics Division, P-25, Los Alamos National Laboratory, Los Alamos, NM 87545, USA*

<sup>2</sup>*Theoretical Division, DDT-DO, Los Alamos National Laboratory, Los Alamos, NM 87545, USA*

(June 11, 1998)

The relativistic hydrodynamical model HYLANDER-C is used to give estimates for single inclusive particle momentum spectra in  $\sqrt{s} = 200 \text{ GeV/nucleon}$  Au+Au collisions that will be investigated experimentally in the near future. The predictions are based on initial conditions that the initial fireball has a longitudinal extension of  $1.6 \text{ fm}$  and an initial energy density of  $30.8 \text{ GeV/fm}^3$  as obtained from a cascade model. For the collision energy considered here, different stopping scenarios are explored for the first time. Our calculations give particle yields of the order of 10,000 to 20,000 charged particles per event.

PACS numbers: 24.10.Jv, 21.65.+f, 24.85.+p, 25.75.-q

Forthcoming experiments at the Relativistic Heavy-Ion Collider (RHIC) at the Brookhaven National Laboratory (BNL) are designed to search for a new state of nuclear matter, the quark-gluon plasma (QGP) [1]. The existence of a QGP should be reflected in the equation of state (EOS) of nuclear matter, which is a relationship between extensive variables, e.g., pressure, energy density, and baryon density.

Those theoretical models such as relativistic hydrodynamics which are capable of describing relativistic heavy-ion collisions *and* which also allow for an explicit use of an EOS have to be based on a thermodynamical approach. Several models based on relativistic hydrodynamics exist (for recent reviews *cf.*, e.g., Refs. [2,3]); these models assume the existence of local equilibrium. In general, the models solve the hydrodynamical equations – which in the case of ideal relativistic fluids are given by the relativistic Euler equations [4] – by sophisticated numerical techniques.

There are essentially only three numerical techniques that are employed in the study of heavy-ion reactions [2]: particle methods, continuum methods, and predictor-corrector methods. In our attempt to make predictions for single inclusive particle momentum spectra of various hadron species emerging from  $\sqrt{s} = 200 \text{ GeV/nucleon}$  Au+Au collisions, we shall use a predictor-corrector model, which has been successful in providing a consistent and coherent description of the single and double inclusive cross sections of mesons and baryons for several types of fixed target heavy-ion collisions at CERN/SPS beam energies near 200 A·GeV: HYLANDER-C [5], which is the upgraded successor of HYLANDER [6].

Predictor-corrector type fluid models begin the calculations with the matter already highly compressed and the numerical code then follows the expansion of the fluid as governed by a particular EOS. At relativistic energies, it is important to employ a covariant description of freeze-out, which allows the calculation of the various particle spectra [7]. In earlier work, the initial state of the hot and dense zone of nuclear matter – the fireball – was parametrized, and was adjusted until a match with observables was established [8]. HYLANDER-C, e.g., can use initial conditions ranging between the extremes defined by the Landau [9] (i.e., complete stopping) and the Bjorken [10] (i.e., minimum stopping through a scaling ansatz) initial conditions.

Conversely, one could also take information about the initial state of the fireball from other sources, e.g., a cascade code, as input and then allow the system to evolve according to an assumed EOS, and finally particle momentum spectra will be calculated. As there are no data yet available for  $\sqrt{s} = 200 \text{ GeV/nucleon}$  Au+Au collisions, we shall discuss in this paper results for a relativistic heavy-ion collision at these high energies using HYLANDER-C, and the sensitivity of observables to different assumptions regarding different initial conditions. For the following we have to specify an equation of state and the initial conditions. In addition we choose for our freeze-out condition a fixed freeze-out energy density,  $\epsilon_f$ , and we assume that the freeze-out occurs for all particle species at the same fixed value of  $\epsilon_f$ . The calculations using HYLANDER and HYLANDER-C which reproduced data of the CERN NA35, NA44 and NA49 collaborations [11] - [13] were obtained while using an EOS with a phase transition to a QGP at a critical temperature  $T_C = 200 \text{ MeV}$  (*cf.* Refs. [14,15], and Refs. therein). The EOS used in this work does not depend on the baryon density (which is a valid assumption for the collision energy regime considered here), and thus the

---

\*E. Mail: schlei@LANL.gov

†E. Mail: dds@LANL.gov

freeze-out energy density translates into a fixed freeze-out temperature  $T_f$ . The choice for the freeze-out temperature has been  $T_f = 139 \text{ MeV}$  in the former calculations; we shall use the same value here. This is consistent with our attempt to be conservative in determining possible results for the Au+Au collisions by choosing exactly the same conditions for the fireball expansion (through the same choice of the EOS) and the same conditions for the freeze-out (through the same choice for  $\epsilon_f$  and  $T_f$ ) that were used in the successful description of the CERN/SPS data.

Because the appropriate initial conditions for the formation of the Au+Au fireball are unknown, we shall adopt values for the hydrodynamical input from K. Geiger's parton cascade calculations [16–18] (other cascade models [19,20] have been employed for predictions of the heavy-ion collision discussed here with results that are similar to K. Geiger's results). In Ref. [17] it was reported that after an equilibration proper time,  $\tau_{eq} = 1.8 \text{ fm}/c$ , the initial fireball originating from a  $\sqrt{s} = 200 \text{ GeV/nucleon}$  Au+Au collision was formed with an initial longitudinal extension (of the Landau volume [21]),  $\Delta = 1.6 \text{ fm}$ , and an upper value for the initial energy density,  $\epsilon_\Delta = 30.8 \text{ GeV}/\text{fm}^3$ .

We use here for the initial distributions the initial condition scenario which has been described in Refs. [21,22]. Specifically, our model uses the five initial parameters,  $K_L$ ,  $\Delta$ ,  $y_\Delta$ ,  $y_m$  and  $\sigma$ , which are the relative fraction of thermal energy in the central fireball, the longitudinal extension of the fireball, the fluid's rapidity at the edge of the central fireball, the fluid's rapidity at the maximum of the initial rapidity distribution of the baryons, and the width of the initial baryonic rapidity distribution, respectively. Furthermore, it is assumed that an initial transverse fluid velocity component is absent, and the initial longitudinal distributions (with respect to the beam axis) for energy density,  $\epsilon$ , and baryon density,  $n_B$ , are smeared out with a Woods-Saxon parametrization in the transverse direction,  $r_\perp$  (*cf.* Refs. [22,23]).

In the following, we keep  $\Delta$  and  $K_L$  fixed to the values provided by K. Geiger's results. We stress that an initial energy density,  $\epsilon_\Delta = 30.8 \text{ GeV}/\text{fm}^3$  in the Landau volume represents only 11.5% of the total available energy. The parameter  $\sigma$  we keep fixed also without loss of generality. In particular, it is our intent to discuss six possible stopping scenarios (*cf.* Table I, scenarios I - VI). We can accomplish this by varying the only two parameters left in our model for the initial conditions,  $y_\Delta$  and  $y_m$ . A larger value for the absolute value of rapidity,  $y_\Delta$ , at  $z = \pm\Delta/2$  results in a larger initial rapidity field,  $y(z)$ , which can be interpreted in having less stopping. Conversely, initially concentrating as much baryonic matter as possible in the central region of the initial fireball as energy conservation permits us, i.e., by minimizing  $y_m$ , results in having a much larger stopping compared to the cases where the baryonic matter lies further outside. For the following

discussion, we have chosen three scenarios where as much baryonic matter as possible is concentrated in the central region of the initial fireball (scenarios I, III, V), and three scenarios where the baryonic matter lies further outside (scenarios II, IV, VI).

In Fig. 1 we show the initial distributions of energy density,  $\epsilon$ , baryon density,  $n_B$ , and the fluid rapidity,  $y_F$ , normalized to their maximum values,  $\epsilon^{max}$ ,  $B_{max}^0$ , and  $y_{cm}$ , and plotted against the longitudinal coordinate  $z$ , for each of the six initial conditions. The absolute values of the initial fluid rapidity,  $y_\Delta$ , at  $z = \pm\Delta/2$  decrease from the top to the bottom of Fig. 1. Therefore, we have a greater amount of stopping as one goes from the top to the bottom of Fig. 1. Comparing the left column of Fig. 1 (scenarios I, III, V) with the right column (scenarios II, IV, VI), we recognize that we have greater stopping when going from the right to the left in the figure. Table I gives also the relative fractions,  $f_{n_B}^\Delta$ , of baryons initially concentrated in the initial fireball volume of length  $\Delta$ . Thus, scenario V gives the highest initial stopping, and scenario II gives the smallest initial stopping.

Inspecting Fig. 1 further, we also see that the initial conditions I and II are closer to a Bjorken-type initial condition, and scenarios V and VI are closer to a Landau-type initial condition.

After fixing the various initial conditions, we allow for expansion and cooling of the relativistic fluids by solving the relativistic Euler equations. As mentioned above, freeze-out occurs for all particle species at the same fixed value of  $T_f = 139 \text{ MeV}$ . In Fig. 2 we display for each scenario the isotherms of the expanding systems at the radial coordinate,  $r_\perp = 0$ . In particular, the outer isotherms represent the freeze-out hypersurfaces at  $r_\perp = 0$ . The total lifetimes,  $t_{max}$ , of the various systems range from  $37.8 \text{ fm}/c$  to  $49.7 \text{ fm}/c$ , and the total lifetimes of the QGP,  $t_{QGP}$ , range from  $16.9 \text{ fm}/c$  to  $23.7 \text{ fm}/c$ . We note that  $t_{QGP}$  is not correlated with  $t_{max}$  because of the complex behaviour of the numerically treated multi-dimensional relativistic fluids. Furthermore, looking at Fig. 2, we can see that the freeze-out hypersurfaces are to a large extent hyperbola-like shaped, which we especially would expect from a purely Bjorken type expansion scenario [10].

Following the formalism which is outlined in refs. [21,22], we have calculated single inclusive particle momentum spectra of pions, kaons, and protons for  $\sqrt{s} = 200 \text{ GeV/nucleon}$  Au+Au collisions. We have taken into account resonance decay contributions up to the third generation of particle production. Figs. 3 and 4 show our results for rapidity and transverse momentum spectra, respectively, for the six initial conditions. It is remarkable that a wide range of shapes is possible for the rapidity spectra. We observe an almost Gaussian distribution for scenario V, a flat rapidity plateau for scenario III, and saddle-shaped distributions for all the other four scenarios. In agreement with expectation, the rapidity spec-

tra are narrower and the transverse momentum spectra show a higher mean transverse momentum,  $\langle k_{\perp} \rangle$ , (i.e., a smaller slope,) for initially higher stopping. Contrary to the common belief [10], Bjorken type expansion scenarios do not necessarily lead to flat rapidity plateaus. This is because of finite size effects of the fireballs.

In addition, we list in Table II the absolute particle yields for some selected particle species. The numbers were obtained by integrating the corresponding rapidity and transverse momentum spectra, respectively. We stress that the particle yields in Table II are obtained while assuming that  $\epsilon_{\Delta} = 30.8 \text{ GeV}/\text{fm}^3$ , i.e.,  $K_L = 11.5\%$ . If one would choose pure Landau initial conditions (i.e., complete stopping) one would obtain approximately 10 times that many particles.

To summarize, we have used the relativistic hydrodynamical model HYLANDER-C to give estimates for single inclusive particle momentum spectra of various hadrons for  $\sqrt{s} = 200 \text{ GeV}/\text{nucleon}$  Au+Au collisions. Our predictions are based on the assumptions that the initial fireball has a longitudinal extension of  $1.6 \text{ fm}$  and an initial energy density of  $30.8 \text{ GeV}/\text{fm}^3$ , values consistent with results obtained using the cascade code of Geiger. Within different stopping scenarios, we have investigated the freeze-out hypersurfaces and the corresponding final particle distributions. Our calculations give particle yields of the order of 10,000 to 20,000 charged particles per event. We have also found that the shapes of the rapidity spectra are sensitive to the assumed stopping power. Our quantitative estimates are based on assumptions for the initial conditions obtained from cascade models, the EOS, and the proper freeze-out conditions for the heretofore experimentally unexplored regime of  $\sqrt{s} = 200 \text{ GeV}/\text{nucleon}$  collisions. Information concerning each of these must be gained with additional theoretical work as well as data when they become available. We are grateful for many instructive discussions with Dr. Klaus Kinder-Geiger. This work has been supported by the U.S. Department of Energy.

- [7] F. Cooper, G. Frye, E. Schonberg, Phys. Rev. **D11**, 192 (1975).
- [8] B.R. Schlei, D. Strottman, N. Xu, Phys. Rev. Lett. **80**, 3467 (1998).
- [9] L.D. Landau, Izv. Akad. Nauk SSSR **17**, 51 (1953).
- [10] J.D. Bjorken, Phys. Rev. **D27**, 140 (1983).
- [11] S. Wenig, Ph.D. thesis, GSI-Report 90-23 (October 1990).
- [12] I. G. Bearden et al. (NA44 Collaboration), Phys. Lett. **B388**, 431 (1996).
- [13] P.G. Jones et al. (NA49 Collaboration), Nucl. Phys. **A610**, 188c (1996).
- [14] K. Redlich, H. Satz, Phys. Rev. **D33**, 3747 (1986).
- [15] U. Ornik, M. Plümer, B.R. Schlei, D. Strottman, R.M. Weiner, Phys. Rev. **C54**, 1381 (1996).
- [16] K. Geiger, and B. Müller, Nucl. Phys. **B369**, 600 (1992).
- [17] K. Geiger, Phys. Rev. **D46**, 4965 (1992); Phys. Rev. **D46**, 4986 (1992); Phys. Rev. **D47**, 133 (1993).
- [18] K. Geiger, and J.I. Kapusta, Phys. Rev. **D47**, 4905 (1993).
- [19] X.-N. Wang, M. Gyulassy, Phys. Rev. **D44**, 3501 (1992).
- [20] M. Gyulassy, X.-N. Wang, Computer Phys. Comm. **83**, 307 (1994).
- [21] J. Bolz, U. Ornik, R.M. Weiner, Phys. Rev. **C46**, 2047 (1992);
- [22] J. Bolz, U. Ornik, M. Plümer, B.R. Schlei, R.M. Weiner, Phys. Rev. **D47**, 3860 (1993).
- [23] J. Sollfrank, P. Huovinen, P.V. Ruuskanen, Heavy Ion Phys. **5**, 321 (1997).

TABLE I. Properties of the initial fireballs.

	I	II	III	IV	V	VI
Initial parameters						
$K_L$	0.115	0.115	0.115	0.115	0.115	0.115
$\Delta [\text{fm}]$	1.6	1.6	1.6	1.6	1.6	1.6
$y_{\Delta}$	0.9	0.9	0.6	0.6	0.3	0.3
$y_m$	1.52	2.00	1.24	1.75	0.88	1.50
$\sigma$	0.4	0.4	0.4	0.4	0.4	0.4
$T_f [\text{MeV}]$	139	139	139	139	139	139
Output						
$y_{cm}$	5.36	5.36	5.36	5.36	5.36	5.36
$\epsilon_{\Delta} [\text{GeV}/\text{fm}^3]$	30.8	30.8	30.8	30.8	30.8	30.8
$\epsilon_{\Delta}^{max} [\text{GeV}/\text{fm}^3]$	40.7	30.8	45.8	30.8	41.8	30.8
$B_{max}^0 [\text{fm}^{-3}]$	2.23	2.09	1.52	1.44	0.78	0.74
$f_{n_B}^{\Delta}$	0.062	0.003	0.055	0.002	0.072	0.001
$t_{max} [\text{fm}/c]$	49.7	51.7	45.6	49.0	37.8	43.5
$t_{QGP} [\text{fm}/c]$	23.7	16.9	23.5	20.3	21.2	20.6

TABLE II. Particle yields of pions, kaons, and protons.

	I	II	III	IV	V	VI
$N_{\pi^+}$	5320	4654	5802	5501	6816	5741
$N_{\pi^-}$	5420	4748	5903	5609	6932	5840
$N_{K^+}$	770	674	834	798	972	822
$N_{K^-}$	709	616	776	735	915	766
$N_p$	328	305	336	352	364	333

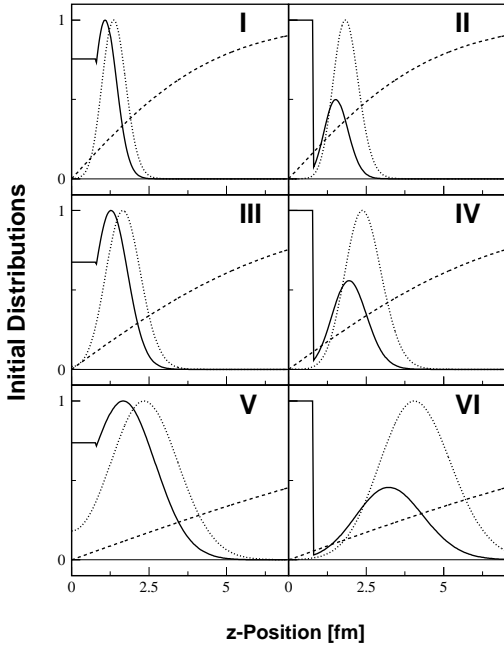


FIG. 1. Initial distributions of energy density,  $\epsilon$  (solid lines), and baryon density,  $n_B$  (dotted lines), as well as the fluid rapidity,  $y_F$  (dashed lines), normalized to their maximum values (cf. Table I) and plotted against the longitudinal coordinate  $z$ .

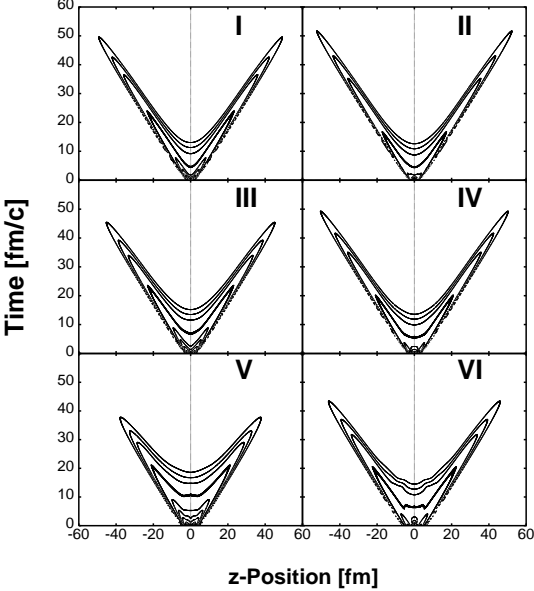


FIG. 2. Thermal evolution of the Au+Au fireballs. In each case the outer contours are isotherms for  $T = 140$  MeV, and each successively smaller contour represents an increase of 20 MeV in the temperature.

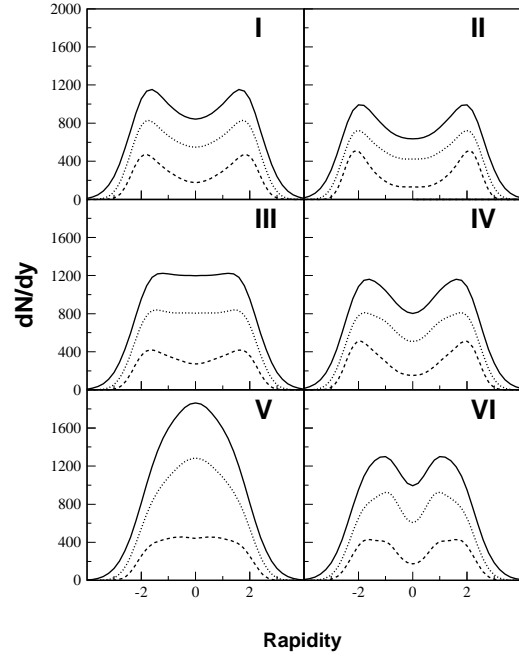


FIG. 3. Rapidity spectra of negative pions,  $\pi^-$  (solid lines), negative kaons,  $K^-$  (dotted lines), and protons,  $p$  (dashed lines). In each plot the rapidity spectra of  $K^-$  and  $p$  are enhanced by a factor of 5 for better visibility.

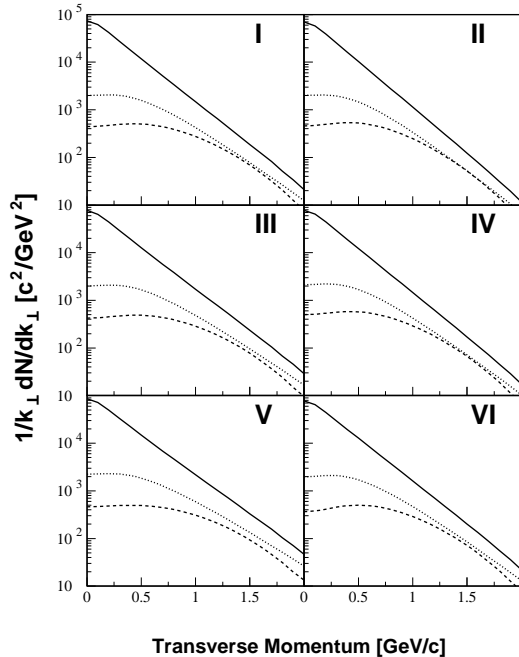


FIG. 4. Transverse momentum spectra of negative pions,  $\pi^-$  (solid lines), negative kaons,  $K^-$  (dotted lines), and protons,  $p$  (dashed lines).